J. Fluid Mech. (1999), *vol.* 383, *pp.* 307–326. Printed in the United Kingdom

Transition from dripping to jetting

By CHRISTOPHE CLANET† AND JUAN C. LASHERAS

Department of Applied Mechanics and Engineering Sciences,
University of California San Diego, La Jolla, CA 92093-0411, USA

(Received 18 March 1997 and in revised form 9 October 1998)

We consider the critical Weber number ($We_c \equiv \rho V_0^2 D/\sigma$) at which the transition from dripping to jetting occurs when a Newtonian liquid of density ρ and surface tension σ is injected with a velocity V_0 through a tube of diameter D downward into stagnant air, under gravity g. We extend Taylor's (1959) model for the recession speed of a free edge, and obtain in the inviscid limit an exact solution which includes gravity and inertia effects. This solution provides a criterion for the transition which is shown to occur at a critical Weber number

$$We_c = 4\frac{Bo_o}{Bo}\left[1 + KBo_oBo - ((1 + KBo_oBo)^2 - 1)^{1/2}\right]^2,$$

where Bo and Bo_o are the Bond numbers $\left(Bo \equiv [\rho g D^2/(2\sigma)]^{1/2}\right)$, respectively based on the inside and outside diameter of the tube, and K is a constant equal to 0.37 for the case of water injected in air. This critical Weber number is shown to be in good agreement with existing experimental values as well as with new measurements performed over a wide range of Bond numbers.

1. Introduction

> A tube, the bore of which is so small that it will only admit a hair (*capilla*), is called a capillary tube. When such a tube of glass, open at both ends, is placed vertically with its lower end immersed in water, the water is observed to rise in the tube, and to stand within the tube at a higher level than the water outside. The action between the capillary tube and the water has been called Capillary Action, and the name has been extended to many other phenomena which have been found to depend on properties of liquids and solids similar to those which cause water to rise in capillary tubes ('Capillary action', by James Clerk Maxwell in the *Encyclopaedia Britannica*).

This introduction by J. C. Maxwell is related to the problem of a liquid dripping out of a tube through Tate's law (1864): *the weight of the drop is in proportion to the weight of water which would be raised in that tube by capillary action.* Obviously, as noticed by Rayleigh (1899) 'Sufficient time must of course be allowed for the formation of the drops; otherwise no simple results can be expected. In Tate's experiments the period was never less than 40 seconds'. If the time is not sufficiently long, instead of a drop by drop emission, one observes the formation of a continuous jet that breaks further downstream due to the Savart–Plateau–Rayleigh's capillary instability.

In this paper, we address the problem of the transition from the drop by drop regime to the continuous jet in the case of a Newtonian liquid of density ρ, kinematic viscosity ν, and surface tension σ injected vertically downward (following the direction

† Present address: Institut de Recherches sur les Phénoménes Hors Equilibre, Université de Provence, Centre de St Jérôme, Service 252, Marseille Cedex 20, France.

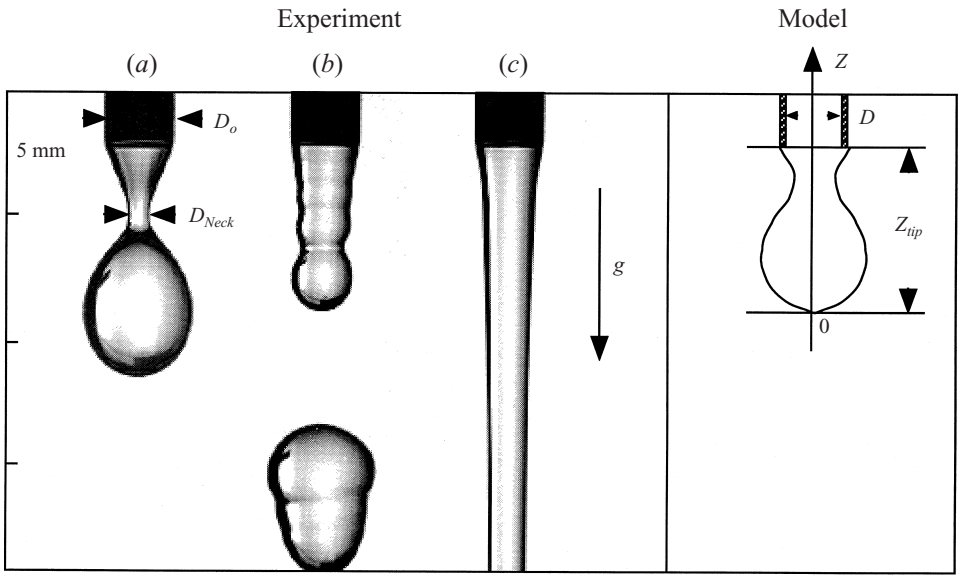

FIGURE 1. Different regimes obtained with $D = 2.159$ mm and $D_o = 2.769$ mm: (*a*) $We = 0.063$, (*b*) $We = 1.73$, (*c*) $We = 2.3$.

of gravity, $\boldsymbol{g}$), into stationary air with a mean velocity V_0 through a needle of internal diameter D and outer diameter D_o. The outer diameter, D_o, or thickness of the tube, is a parameter of our study since the water always wets the stainless steel needle we used. In the unwetting limit, D is the only geometrical parameter.

In terms of non-dimensional parameters, we are addressing the problem of finding the critical Weber number $We_c \equiv \rho V_0^2 D/\sigma$ at which the transition takes place. Several regimes are observed prior to this transition:

(i) For $We \ll 1$, drops with constant mass M periodically detach from the nozzle at a constant frequency (see figure 1*a*). This regime, in which the droplets detach from the nozzle at a downstream distance of approximately one diameter, is referred to as *Periodic Dripping* (*PD*). It was first studied by Tate (1864), a pharmacist, who, by simply equating surface tension forces to gravity forces at the point of detachment, found that the mass of the drop that detaches is $M = 2\pi\sigma R_o/g$, where $R_o = D_o/2$ is the external radius. Thirty-five years later, Rayleigh (1899), while emphasizing the difficulties involved in the theoretical calculation of the mass that detaches from a nozzle, conducted a dimensional analysis (also reported in Rayleigh 1915) proposing that $M = (\sigma R_o/g) f(R_o/a)$, where f is a function that can be determined experimentally and $a \equiv (2\sigma/(\rho g))^{1/2}$, is the capillary length ($a \approx 3.8$ mm for water). Using the measurements he made with the assistance of Mr Gordon, he found that $f(R_o/a)$ can be approximated by a constant equal to 3.8 (instead of the value 2π predicted by Tate's law). Twenty years later, Harkins & Brown (1919) published their landmark paper, *the determination of surface tension, and the weight of falling drops*. Their measurements obtained with water and benzene ($\rho_{benzene} = 881\ \mathrm{kg\,m^{-3}}$, $\sigma_{benzene} = 0.029\ \mathrm{kg\,s^{-2}}$ and $a_{benzene} = 2.58$ mm), over the range $0.257 < R_o/a < 2.625$ showed that $f(R_o/a)$ is better correlated by a third-order polynomial with a relative minimum at $R_o/a \approx 1$ and a relative maximum at $R_o/a \approx 2$. The high accuracy of their measurements led to the well known 'drop-weight' method to determine the surface tension of a liquid. This set of careful experiments was further

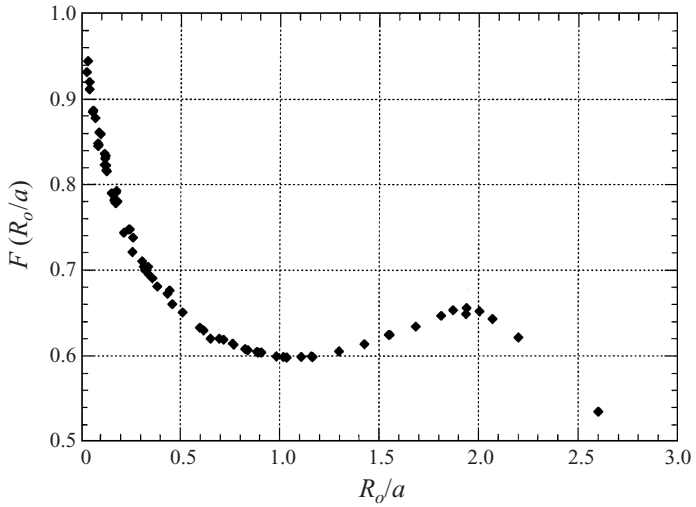

FIGURE 2. Harkins & Brown factor.

extended to the case of orifice diameters much smaller than the capillary length, $0.0276 < R_o/a < 0.4463$, and to a wide range of fluid viscosities and surface tensions by Wilkinson (1972). The correlation function $F = f(R_o/a)/(2\pi)$ obtained by these authors is shown in figure 2, and is usually referred to as the *Harkins and Brown factor* or F_{HB}. In the limit of $R_o/a \ll 1$, the drops are nearly spherical, and one recovers Tate's law with $F_{HB} = 1$. However, when R_o/a increases, the equilibrium shape of the pendant drop prior to its detachment deviates progressively from sphericity, and the function F_{HB} takes the cubic dependency on R_o/a shown in figure 2. In the limit $R_o/a \ll 1$, perturbative theoretical methods have been used to approach $F(R_o/a)$ (Chesters 1977). Other theoretical studies have dealt with the pendant drop problem (Michael 1981; Padday & Pitt 1973), some of which deal with the special case of very viscous fluids (Wilson 1988). In all these studies, inertia effects were neglected and the quasi-steady assumption was used.

(ii) As the Weber number is increased, a first threshold is reached, above which the dripping process continues but the masses of the detaching drops begin to vary from one to the next in a quasi-periodic or chaotic way (figure 1*b*). This second dripping regime, which only occurs in a narrow range of exit velocities, is often referred to as the *Dripping Faucet* (*DF*), and has been studied extensively as an example of a nonlinear dynamical system exhibiting a chaotic attractor (Martien *et al.* 1985; D'Innocenzo & Renna 1996).

(iii) By further increasing the Weber number, a second threshold is reached, where the detachment point of the droplets suddenly moves downstream from the exit of the nozzle (typically to a distance greater than 10*D*), and a continuous jet is formed (figure 1*c*). This second threshold identifies the transition from dripping to jetting. In this third regime, hereafter referred to as the *Jetting Regime* (*J*), the liquid jet that exits the nozzle undergoes the capillary instability whereby droplets are formed further downstream. This instability was first studied experimentally by Savart (1833) and theoretically by Plateau (1873) but is still often referred as the Rayleigh instability (Rayleigh 1879).

Although the periodic dripping (*PD*), chaotic dripping (*DF*) and jetting (*J*) regimes have all been studied extensively, the transition from one to the other has received

much less attention. Without recognizing the existence of the two dripping regimes described above, the transition from dripping to jetting was first studied by Smith & Moss (1917). These authors and subsequent others (Tyler & Richardson 1925; Tyler & Watkin 1932) focused on the variation of the jet length with the injection velocity and identified two critical velocities, the lowest one corresponding to the transition from dripping to jetting, and the second upper one to the transition from a laminar to a turbulent jet. They concluded that the threshold velocity for the transition to jetting was given by $V_J = K(\sigma/(\rho D))^{1/2}$, where the 'constant' K was found to vary in their experiments from 2.5 to 3.5. In liquid–liquid systems, the transition was further studied (see Clift, Grace & Weber 1978 and McCarthy & Molloy 1974) and several expressions for the drop volume that detaches and for the jetting velocity were proposed by Scheele & Meister (1968*a*,*b*) and Kumar (1971).

Recently following the conjecture of Monkewitz (1990) that the transition from jetting to dripping could be related to a global instability, Le Dizès, (1997) has conducted a global linear stability analysis of falling capillary jets in the limit $V_0 D/\nu \gg 1$ and $V_0^2/(gD) \gg 1$. In this limit, the author shows that if the basic jet has approximately an axisymmetric plug profile, it becomes locally absolutely unstable at the orifice for a critical value of the Weber number $We = \rho V_0^2 D/\sigma \approx 6.25$.

The problem of determining the conditions at which the transition takes place over the whole range of tube diameters and liquid properties is a rather complex one. In this paper, we restrict our study only to the cases where:

(*a*) the inner diameter of the tube is small enough for the liquid interface to be stable to the Rayleigh–Taylor instability;

(*b*) inertia, capillary and gravitational effects are dominant over the viscous forces, and the problem can be treated in the inviscid limit;

(*c*) the thickness of the tube $(D_o - D)$, is sufficiently small for the liquid exiting the tube to wet the entire section, in which case D_o fixes the characteristic length for the capillary effect.

In the Bond number parameter space shown in figure 3 ($Bo \equiv D/a$), the region in which our study is performed corresponds to the hatched area given by the coordinates $l_v/a < Bo < \pi/\sqrt{2}$ and $(Bo_o - Bo) < 2\pi$. The upper limit of Bo is given by the critical diameter above which the tube is unstable to Rayleigh–Taylor instability. This limit can be estimated from the dispersion relation $\omega(k) = (kg - \sigma k^3/\rho)^{1/2}$ which gives a marginal wavenumber $k_c = 2\pi/\lambda_c = (\rho g/\sigma)^{1/2}$. Taking $\lambda_c \approx 2D$, one obtains the upper limit of the Bond number as $Bo_c = \pi/\sqrt{2}$. For water, this corresponds to a diameter $D = 8$ mm. Above this limit, air enters the tube and changes the problem. The lower Bond number limit is given by the diameter below which viscous forces can no longer be neglected. In our problem, viscous effects act on a time scale $t_v \sim D^2/\nu$ and the gravitational effect on the time scale $t_g \sim (D/g)^{1/2}$. In the inviscid limit, $t_g \ll t_v$, which gives $D \gg l_v$, where $l_v \equiv (\nu^2/g)^{1/3}$. The lower Bond number of our study is thus given by $Bo = l_v/a$ (in the case of water, $l_v = 46$ μm and $Bo = 1.23 \times 10^{-3}$).

The upper limit of the vertical axis is given by the tube thickness $(D_o - D)$ above which the liquid does not wet the tube entire exit section. From the study of Limat *et al.* (1992), we estimate the value of this limit as $D_o - D = 2\pi a$, which gives $Bo_o - Bo = 2\pi$ (in the case of water, this condition limits the thickness of the tubes to $D_o - D < 2.3$ cm).

Section 2 describes the experimental set-up. The experimental results are given in § 3 followed by the presentation of the models in §§ 4 and 5. The conclusions are presented in § 6.

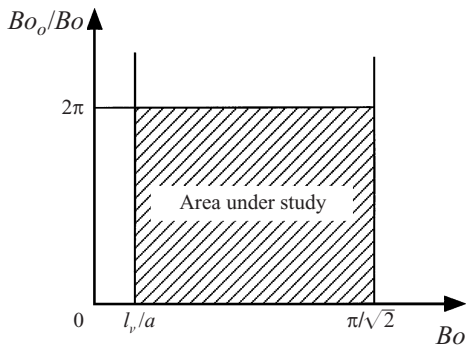

FIGURE 3. Domain under consideration in the Bond number space.

ρ(kg m^{-3})	v(m^2 s^{-1})	σ(kg s^{-2})	a(m)	l_v (m)
1000	10^{-6}	0.073	3.8×10^{-3}	50×10^{-6}

TABLE 1. Physical properties of deionized water at 22 °C.

2. Experimental set-up

All the reported experiments were performed using deionized water at room temperature (22 °C), the properties of which are recalled in table 1, where v is the kinematic viscosity. The deionized water was supplied to the nozzle at a constant pressure through a regulator and a flowmeter. The nozzles consisted of cylindrical, stainless steel hypodermic needles with length/diameter ratios $L/D > 50$. The external diameter, D_o, is not varied independently from D but is fixed by the thickness of the material used to make the needles. The relation between D_o and D, in m, can be approximated by the third-order polynomial $D_o = M_0 + M_1 D + M_2 D^2 + M_3 D^3$ with $M_0 = 4.16 \times 10^{-5}$ m, $M_1 = 1.83$, $M_2 = -501$ m^{-1} and $M_3 = 1.01 \times 10^5$ m^{-2}. The control parameters of the experiments are the nozzle's inner diameter D, and the jet's mean exit velocity V_0, defined as the ratio of the mean exit flow rate to the exit cross-section area. The mean exit flow rate was measured with an accurate rotameter (110 units corresponding to 2 cm^3 s^{-1}), while the exit velocity profile was estimated assuming a fully developed pipe flow. The range of variation of the control parameters (D,V_0) and the corresponding Weber ($We \equiv \rho V_0^2 D/\sigma$) and Reynolds ($Re \equiv V_0 D/v$) numbers are reported in table 2, where V_J is the velocity corresponding to the transition from dripping to jetting and V_1 to the minimum value tested. Since the Reynolds numbers never exceed 600, the velocity profiles were always taken as parabolic. It is to be noted that all the cases studied here correspond to needles whose thicknesses are much smaller than the capillary length, and the corresponding Bond numbers are always within the region indicated in figure 3.

The drop formation was observed experimentally with a high-speed video camera Kodak-Ektapro1000, (with a pixel array resolution of 192 rows $\times$ 240 columns) able to run 1000 f.p.s. full frame and 6000 f.p.s. with a 32 $\times$ 240 reduced matrix. High acquisition rates were used to fully resolve the time evolution of the neck, $D_{Neck}(t)$ (figure 1) and it was adjusted from experiment to experiment to ensure an accurate resolution of the characteristic time (typically 100 frames to describe the necking). The

D (mm)	D_o (mm)	V_1 (m s^{-1})	V_J (m s^{-1})	We_1 ($\times 10^{-5}$)	We_J	Re_1	Re_J
0.24100	0.508	0.0095	1.35	30	6.0	2.3	325
0.31800	0.635	0.0072	1.2	20	6.3	2.3	382
0.39400	0.711	0.0043	1.06	10	6.1	1.7	417
0.49500	0.813	0.0034	0.95	8	6.1	1.7	470
0.58400	0.902	0.0039	0.87	10	6.0	2.3	508
0.83800	1.27	0.0016	0.60	3	4.1	1.3	503
1.1900	1.65	0.0021	0.45	7	3.3	2.5	535
1.6000	2.11	0.0012	0.33	3	2.4	1.9	528
2.1600	2.77	0.00062	0.25	1	1.8	1.3	540
4.1000	4.75	0.00024	0.11	0.3	0.7	0.98	451

TABLE 2. Range of variation of the relevant parameters.

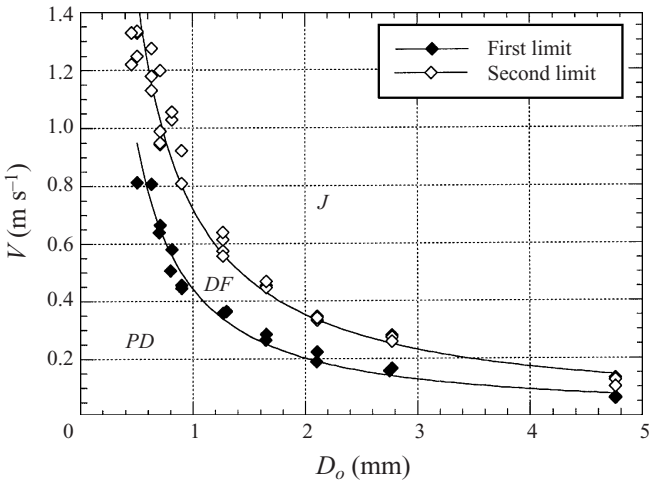

FIGURE 4. Boundaries of the different domains.

resulting frames were processed with the NIH image 1.60 image processing package and further analysed with Matlab.

3. Experimental results

3.1. *Transitions and hysteresis effects*

The critical velocities separating the three different regimes PD, DF and J are presented in figure 4 for the range of diameters tested. The reported transitions were obtained by gradually increasing the flow rate from PD to J. The first limit was defined as the threshold velocity for which the droplet emission changed from periodic to quasi-periodic. This was experimentally determined as the velocity (V_{DF}) for which the size of the emitted drop changed from one period to the next by a value larger than 20%. The second threshold was defined as velocity (V_J) for which the point of drop detachment suddenly moved from a downstream location of a few diameters to a distance greater than $10D_0$.

One could expect that these thresholds should be different when starting from the jetting regime and decreasing the flow rate. Table 3 reports the two transition

D (mm)	D_o (mm)	V_J^+ (m s^{-1})	V_J^- (m s^{-1})
0.241	0.508	1.35	1.35
0.318	0.635	1.2	1.2
0.394	0.711	1.06	1.06
0.495	0.813	0.95	0.95
0.584	0.902	0.87	0.82
0.838	1.27	0.60	0.60
1.19	1.65	0.45	0.43
1.60	2.11	0.33	0.29
2.16	2.77	0.25	0.19
4.10	4.75	0.11	0.070

TABLE 3. Quantification of the hysteresis effect.

velocities, from dripping to jetting (V_J^+), and from jetting to dripping (V_J^-). The experimental accuracy of these measured thresholds is estimated to be 10%, according to the repeatability of the results. For small nozzle diameters, the hysteresis effect is negligible. However, it becomes clear for nozzle diameters of the order of or larger than the capillary length ($D_o \geqslant 1.6$ mm). This hysteresis effect will be addressed later in § 5.

3.2. *The period of drop emission*

For a given diameter, starting with $V_0 \approx 0$, one first observes the PD regime where the period between drop emissions is constant and the point of detachment is close to the nozzle's exit (typically $1D_o$), as shown in figure 1. A typical time evolution of Z_{tip}/D_o, measured in this region, is shown in figure 5. A study of this regime showing a similar characteristic evolution was done by Longuet-Higgins, Kerman & Lunde (1991). It is observed that when the drop detaches, the portion of the liquid that remains attached to the nozzle oscillates with a characteristic frequency:

$$f_c = \left(\frac{8\sigma}{3\pi\rho\mathscr{V}}\right)^{1/2}, \tag{3.1}$$

where $\mathscr{V}$ is the volume of the remaining portion (see the magnified part of figure 5). As this remaining volume grows steadily due to the constant flow rate, the oscillations are observed to decrease in frequency and to damp out by viscosity at a rate $1/\tau_d \sim (2\pi f_c \nu)^{1/2}/\mathscr{V}^{1/3}$. In the example shown in figure 5, the order of magnitude of the frequency is estimated as $f_c \approx 100$ Hz, and the damping time as $\tau_d \approx 70$ ms. Taking $\mathscr{V} \approx \pi D_o^3/6$ in (3.1) one gets $f_c \approx 112$ Hz and $\tau_d \approx 64$ ms, which are in good agreement with the measured values.

By increasing V_0, one reaches the *first threshold limit* V_{DF} (figure 4) above which the time between emitted drops is no longer constant, but the point of detachment still remains close to the nozzle (between $3D_o$ and $5D_o$). A typical example of time evolution of Z_{tip}/D_o, in this DF regime, is shown in figure 6. In this particular example, we can clearly identify two frequencies, corresponding to the alternate emission of a big and a small drop (figure 1*b*). Usually, we enter the DF regime via a period-doubling bifurcation. It should be noticed that even if the time between drops is no longer constant in this second regime, if the time of detachment is plotted as a function of the drop detachment number, the data can be well fitted to a line, as shown in figure 7. This indicates that in the DF regime, we are still able to define

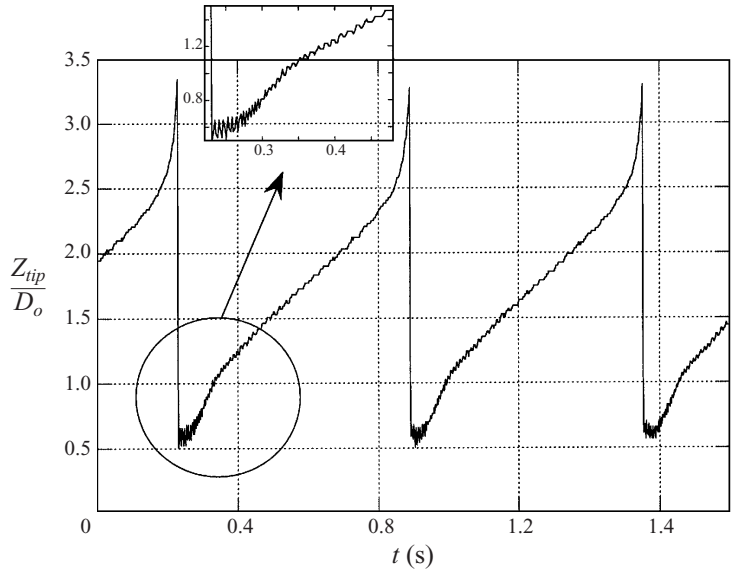

FIGURE 5. Temporal evolution of Z_{tip}/D_o ($D = 1.6$ mm , $D_o = 2.108$ mm , $We = 0.0045$).

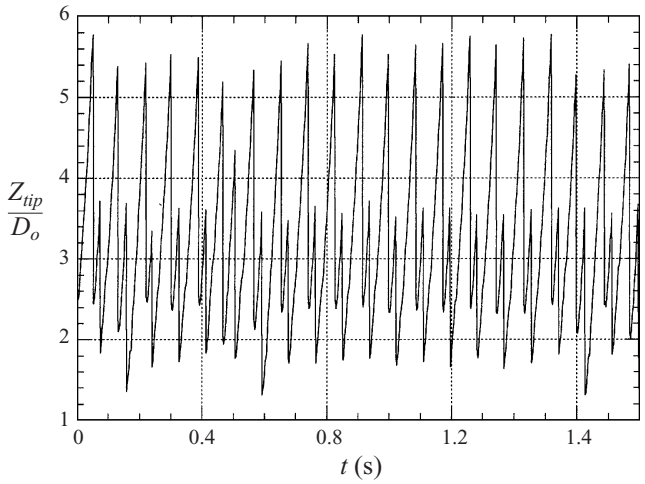

FIGURE 6. Time evolution of Z_{tip}/D_o in the DF regime ($D = 1.6$ mm, $D_o = 2.108$ mm, $We = 1.6$).

a mean period of emission T, corresponding to the slope of this line (in the case presented in figure 7, $T \approx 42.6$ ms). Figure 8 shows the measured period of emission, T, as a function of the Weber number for different diameters tested. It clearly shows that at a given Weber number, the period increases as the diameter is decreased. In the range $We < 1$, the period decays as $We^{-1/2}$. When the Weber number becomes of order unity, inertia effects contribute to a much faster decay of T with the Weber number. Eventually, the transition occurs, at $We \approx 1$ for $D = 4.1$ mm and at $We \approx 6$ for $D = 0.495$ mm. By further increasing the flow rate, we reach the *second threshold limit* V_J (figure 4) where the point of detachment of the first drop moves away from the nozzle (typically to a distance larger than 10 outer diameters), and a continuous jet forms.

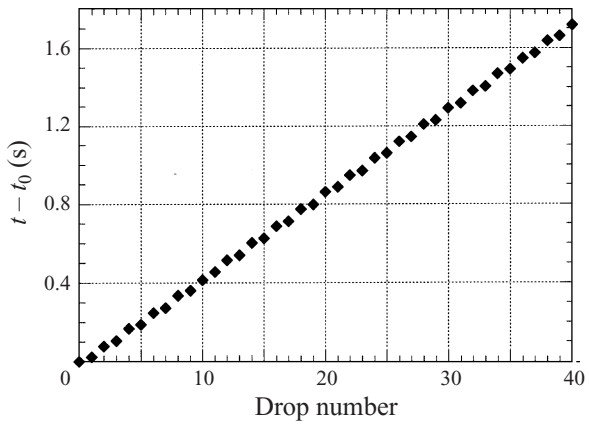

FIGURE 7. Time of detachment presented as a function of the drop number for the case presented in figure 6 (the first drop is referred to as 0 and the corresponding time is t_0).

3.3. *The necking time*

In the dripping mode, the detachment of a drop from the nozzle occurs via the formation of a neck which quickly narrows down until the drop pinches off (figure 1). This process is known as necking, and typically takes only a fraction of the emission time between droplets. For a given set of fluids (in our case water and air), the characteristic time for the necking, τ_n, is only a function of the nozzle's diameter ($\tau_n = G(D_o)$), and this function G can be determined experimentally by measuring the evolution of the diameter of the neck $D_{Neck}(t)$ over a wide range of nozzle diameters. Examples of these measurements obtained through high-resolution video images taken at 1000 frames per second are shown in figure 9. Observe that the smaller the diameter, the shorter the time it takes for the drop to detach. Believing that once the drop is formed, it detaches by some mechanism of instability (Wilson 1988; White & Ide 1975), we fit all our data on the evolution of the necking diameter with an exponential function of the form

$$\frac{D_{Neck(t)}}{D_o} = 1 - \mathrm{e}^{(t-t_0)/\tau_n}, \tag{3.2}$$

where t_0 is a time shift resulting from the fact that the exponential decay is only expected to apply at the onset of the instability and not during the strong nonlinear regime. This function tends to 1 for $t \to -\infty$ and is 0 at $t = t_0$. In all our measurements, the time shift was always kept smaller than τ_n. An example of this fit corresponding to the case of $D_o = 0.902$ mm is shown in figure 10, where we estimate $1/\tau_n \approx 205\ \mathrm{s}^{-1}$, and $t_0 \approx 0.002$ s. Applying the above method to the entire range of diameters tested, we determined experimentally the function $1/\tau_n(D_o)$ which is shown in figure 11.

4. A model for the necking

Let us consider the situation shown in figure 12 where a drop is at the point of detachment. When it detaches, the radial velocity of the neck, V_{Neck} (figure 12), induces a dynamic pressure ρV_{Neck}^2 that is of the same order of magnitude as the capillary action σ/R_o, where $R_o = D_o/2$.

This simple dimensional analysis leads to an estimate of the necking velocity as $V_{Neck} \sim [\sigma/(\rho R_o)]^{1/2}$. The necking time can then be evaluated as $\tau_n \sim R_o/V_{Neck}$, that

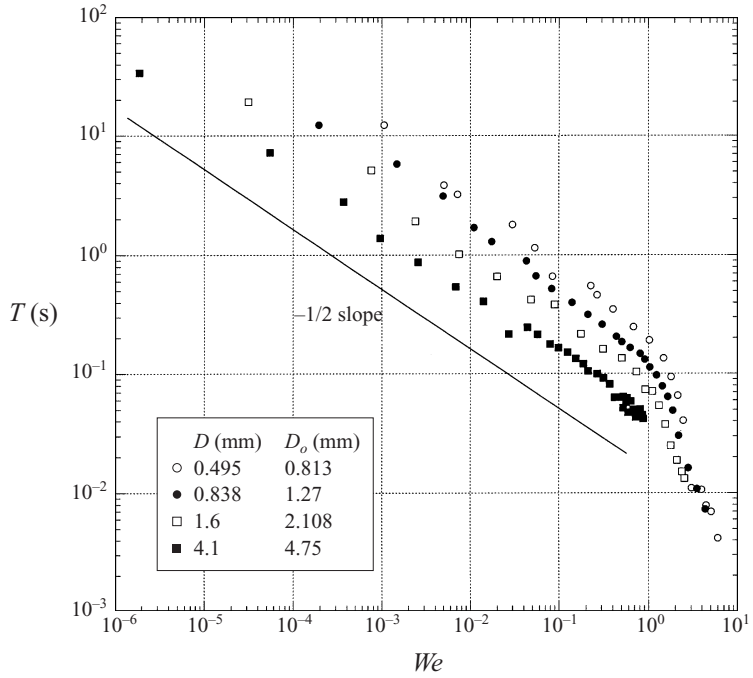

FIGURE 8. Evolution of the period of drop emission as a function of the Weber number.

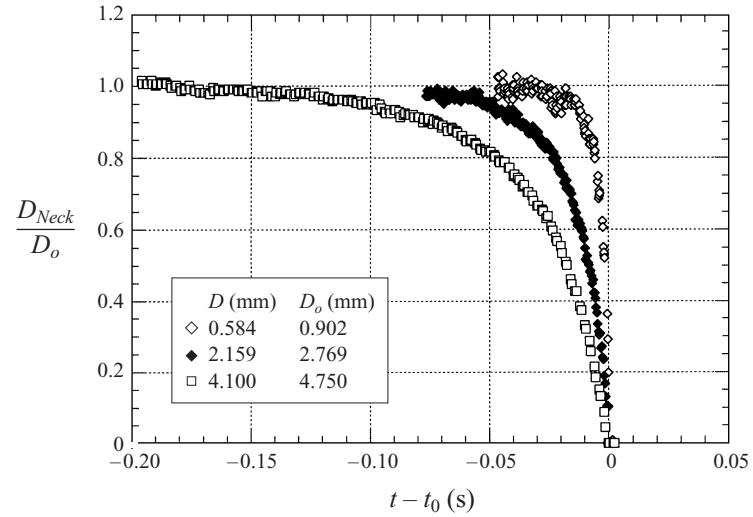

FIGURE 9. Time evolution of D_{Neck} for different outside diameters.

is $\tau_n \sim [\rho R_o^3/\sigma]^{1/2}$ (Eggers & Dupont 1994). In figure 13, we present the necking time measured experimentally, from the preceding section as a function of $[\sigma/(\rho R_o^3)]^{1/2}$. Note that the slope 0.326, obtained by the linear regression, is very close to the value 0.34 given by Rayleigh (1879) for the growth rate of the more unstable wavelength of an inviscid liquid cylinder in air. To test the possibility that the necking instability could be related to the Rayleigh instability, we also conducted experiments with air bubbles released under water, vertically upward, through the same set of tubes.

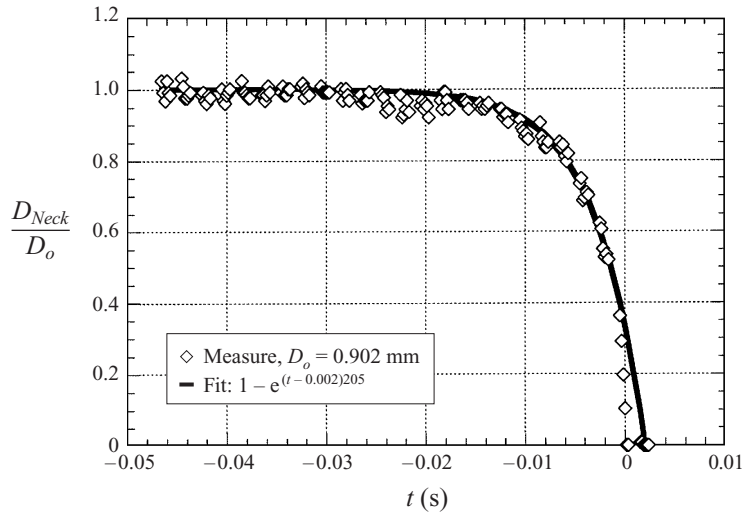

FIGURE 10. Example of exponential fit applied to the time evolution of the neck.

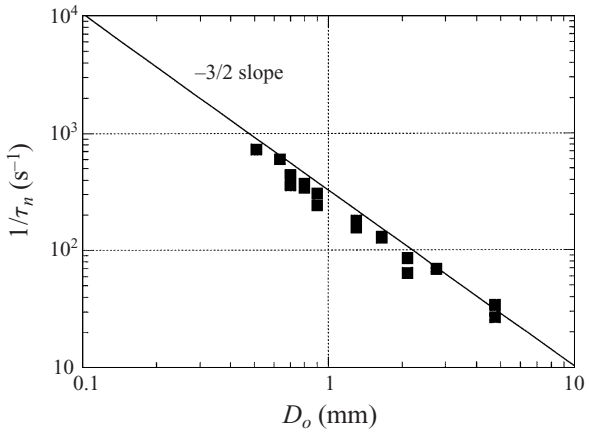

FIGURE 11. Variation of the necking time as a function of the diameter.

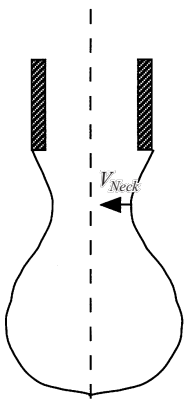

FIGURE 12. Sketch of the detachment.

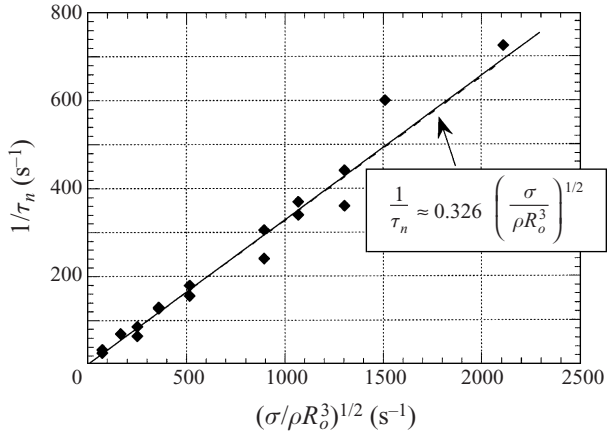

FIGURE 13. $1/\tau_n$ as function of $[\sigma/(\rho R_o^3)]^{1/2}$.

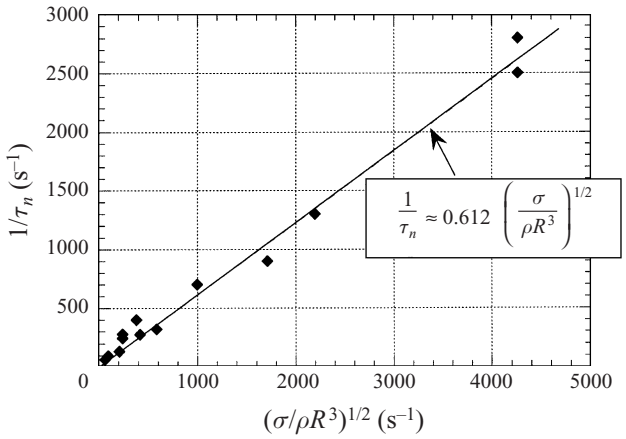

FIGURE 14. $1/\tau_n$ as function of $[\sigma/(\rho R^3)]^{1/2}$ for the bubble case.

The measurements of this second case are presented in figure 14. In the bubble case there is no wetting and the internal diameter D, or radius $R = D/2$ was used as the characteristic length of the problem, instead of D_o. The value 0.612 obtained from the linear regression of these data is higher than that corresponding to the case of the drops but still lower than the value 0.82 predicted for the growth rate of Rayleigh instability of an air cylinder in water.

5. A model for the transition from *PD* to *J*

5.1. *The model*

After a drop is emitted from the tube, the edge of the remaining liquid after the pinching off of the drop begins to recede under the strong pull of surface tension forces as shown in figure 15. As the tip recedes with a velocity $v = \mathrm{d}z/\mathrm{d}t$ a drop of mass M begins to form. The dynamics of this recession can be described with an extension of Taylor's (1959) model for the recessing motion of a rim. The equation

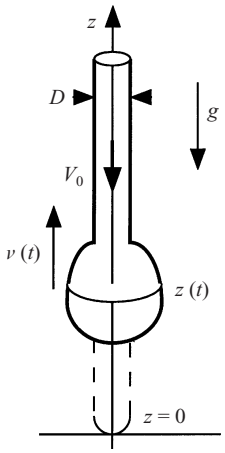

FIGURE 15. Dynamic of a pendant drop.

of motion of the pendant drop can then be written as

$$\frac{\mathrm{d}}{\mathrm{d}t}\left(M\frac{\mathrm{d}z}{\mathrm{d}t}\right) = -Mg + \pi D_o\sigma - \rho S\tilde{V}_0(v + \tilde{V}_0), \tag{5.1}$$

where t represents time, $S \equiv \pi D^2/4$ the cross-section of the jet and $\tilde{V}_0 \equiv |V_0|$ the absolute value of the jet velocity. It simply states that the momentum of the drop changes due to the combined action of gravity, surface tension (which is evaluated on the external diameter) and jet momentum. Since at $t = 0$, the drop is formed at $z = 0$ and initially $M = 0$, the conservation of mass gives

$$M = \rho S\left(z + \tilde{V}_0 t\right), \tag{5.2}$$

and (5.1) reduces to

$$\frac{1}{2}\frac{\mathrm{d}^2z^2}{\mathrm{d}t^2} + \tilde{V}_0\frac{\mathrm{d}z}{\mathrm{d}t} + \tilde{V}_0 t\frac{\mathrm{d}^2z}{\mathrm{d}t^2} = -gz - \tilde{V}_0 tg + \frac{4\sigma D_o}{\rho D^2} - \tilde{V}_0\frac{\mathrm{d}z}{\mathrm{d}t} - \tilde{V}_0^2, \tag{5.3}$$

which has an exact solution given by

$$z(t) = -\tfrac{1}{2}\gamma t^2 + \left(\tilde{V} - \tilde{V}_0\right)t, \quad \text{where,} \quad \gamma = g/3 \quad \text{and} \quad \tilde{V} = \left(\frac{4\sigma D_o}{\rho D^2}\right)^{1/2}. \tag{5.4}$$

The parabolic behaviour of $z(t)$ is summarized in figure 16. On this trajectory of the drop, the point of detachment is identified as z_{max}, where inertia and gravity effects start to overcome surface tension effects. The validity of this solution is discussed in § 5.2. What is important for the model of the transition, is that (5.4) is exact and physical in the domain $t \in [0, t_{max}/2]$, that is until the drop reaches z_{max}. In the limit $g = 0$ and $V_0 = 0$, the above solution shows that the drop moves with the constant velocity $\tilde{V}$ which is similar to the result obtained by Taylor.

With this model, the period of emission, T, is defined as the time needed to fill the volume that the drop will reach prior to detachment. With the above notation, this condition takes the form $\tilde{V}_0 T = z_{max}$ which leads to

$$\frac{Tg}{\tilde{V}} = \frac{3}{2}\frac{\tilde{V}}{\tilde{V}_0}\left(1 - \frac{\tilde{V}_0}{\tilde{V}}\right)^2. \tag{5.5}$$

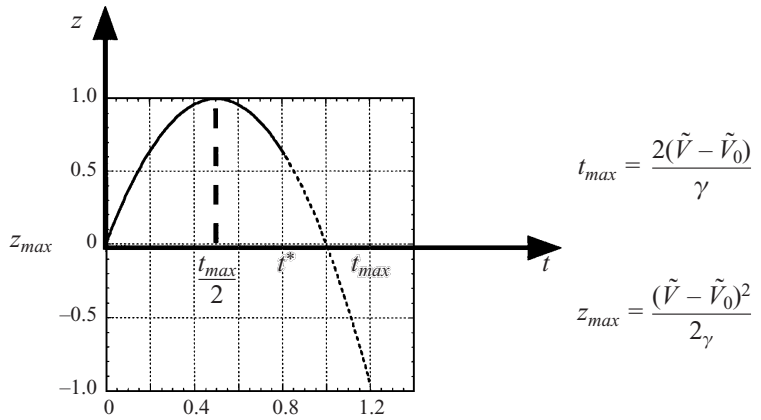

FIGURE 16. Parabolic behaviour of $z(t) = -\gamma/2t^2 + (\tilde{V} - \tilde{V}_0)\, t$.

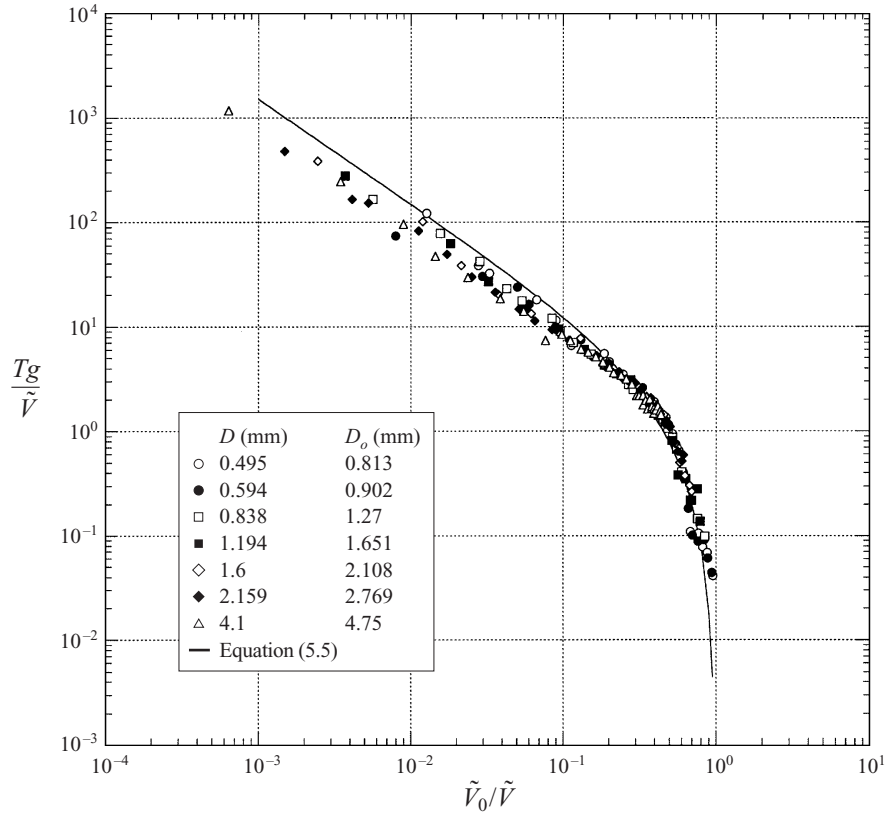

FIGURE 17. Comparison of the calculated period with the experimental results.

The measured period of emission scaled with $\tilde{V}/g$ is plotted in figure 17 against the injection velocity, $V_0/\tilde{V}$, showing not only a remarkable collapse for all the diameters tested, but also an excellent agreement with the prediction given by (5.5). This agreement is particularly good in the region of the transition where $\tilde{V}_0/\tilde{V} \to 1$.

Concerning the transition from dripping to jetting, when the drop detaches, we

Bo	Bo_o	$\tilde{V}$ (ms^{-1})	τ_n (s)	γ (m s^{-2})	$\gamma\tau_n/\tilde{V}$	V_J^+ (m s^{-1})	$\tilde{V}_J$ (m s^{-1})	Error (%)
0.062	0.131	1.598	0.00149	3.27	0.003	1.4	1.47	5.5
0.082	0.164	1.354	0.00209	3.27	0.005	1.2	1.22	2.0
0.102	0.184	1.156	0.00247	3.27	0.007	1.06	1.02	3.0
0.128	0.210	0.984	0.00303	3.27	0.010	0.95	0.85	10.0
0.151	0.234	0.878	0.00354	3.27	0.013	0.87	0.75	13.7
0.217	0.329	0.726	0.00591	3.27	0.026	0.60	0.58	3.4
0.308	0.427	0.583	0.00876	3.27	0.049	0.45	0.42	4.6
0.414	0.547	0.490	0.0126	3.27	0.084	0.33	0.33	0.1
0.560	0.718	0.416	0.0190	3.27	0.149	0.25	0.24	3.2
1.063	1.231	0.287	0.0428	3.27	0.487	0.11	0.11	1.0

TABLE 4. Comparison of the calculated jetting velocity $\tilde{V}_J$ with the experimental values V_J^+.

have shown that it takes a time τ_n to pinch off. During this time, the point of detachment travels down a distance $l_d \approx \tilde{V}_0\tau_n$. When the maximum length reachable by the drop, z_{max}, is greater than l_d, the drop remains attached to the nozzle's exit and then detaches when the critical mass $M_{max} = 2\rho S z_{max}$ is reached. However, when the maximum distance reachable by the drop, is less than this detachment distance, the drop moves progressively downward from cycle to cycle and the jet is formed. Thus, the critical condition for the transition is identified as the condition for which $z_{max} = l_d$. Using (5.4), this condition leads to the relation

$$\left(\frac{\tilde{V}_J}{\tilde{V}}\right)^2 - 2\frac{\tilde{V}_J}{\tilde{V}}\left(1 + \frac{\gamma\tau_n}{\tilde{V}}\right) + 1 = 0 \quad \text{with} \quad \tau_n \approx 3.16\left(\frac{\rho D_o^3}{8\sigma}\right)^{1/2}. \tag{5.6}$$

This equation admits two positive solutions, one bigger than 1 and the other smaller than 1. In our model, the maximum receding velocity of the drop is $\tilde{V}$, so that 1 is the upper limit of the transition. The solution smaller than 1 is thus the only physical solution and it takes the form

$$\frac{\tilde{V}_J}{\tilde{V}} = 1 + \Delta - ((1+\Delta)^2 - 1)^{1/2} \quad \text{where} \quad \Delta \equiv \frac{\gamma\tau_n}{\tilde{V}}. \tag{5.7}$$

In terms of Weber and Bond numbers (5.7) takes the form

$$We_c = 4\frac{Bo_o}{Bo}\left[1 + KBo_oBo - \left((1+KBo_oBo)^2 - 1\right)^{1/2}\right]^2 \text{ with } K \approx 0.372. \tag{5.8}$$

This expression for the jetting velocity is compared to the experimental value in table 4, where V_J^+ is the measured value and $\tilde{V}_J$ the calculated value. Note that the error, presented in the last column, is confined to a few percent for the whole range of diameters. Expression (5.8) can also be compared to the results of Scheele & Meister (1968*a*) who provide some jetting velocities for different liquid–liquid systems and different diameters of nozzles. In their experiment, the lighter fluid 1 is injected from below into fluid 2. To make the comparison, we define the reduced gravity $g' = |\rho_1 - \rho_2|/\rho_1 g$, and assume that the necking time is given by $\tau_n \approx 3.16[8\sigma/(\rho_1 D^3)]^{1/2}$. Furthermore, wetting effects at the nozzle are neglected so that $\tilde{V} = [4\sigma/(\rho_1 D)]^{1/2}$. The comparison is presented for the cases where $\gamma\tau_n/\tilde{V} < 0.5$, a condition that will be discussed in § 5.2. The first column of table 5 refers to the system number as defined by Scheele & Meister. The column V_{JSM} is the transition velocity measured

N	*Bo*	ρ_1 (kg m^{-3})	ρ_2 (kg m^{-3})	μ_1 (kg m s^{-1})	μ_2 (kg m s^{-1})	V_{JSM} (m s^{-1})	$\tilde{V}_J$	Error (%)
1	0.16	683	996.0	0.00039	0.000958	0.40	0.44	9
1	0.33	683	996.0	0.00039	0.000958	0.26	0.28	6
1	0.52	683	996.0	0.00039	0.000958	0.20	0.19	5
1	0.68	683	996.0	0.00039	0.000958	0.16	0.15	10
2	0.27	683	1254	0.00039	0.515	0.32	0.35	8
3	0.26	683	1236	0.00039	0.168	0.32	0.34	6
4	0.28	683	1224	0.00039	0.0785	0.32	0.32	0
5	0.26	683	1190	0.00039	0.0219	0.28	0.34	18
6	0.24	683	1143	0.00039	0.00695	0.32	0.35	10
6	0.75	683	1143	0.00039	0.00695	0.14	0.14	2
7	0.54	836	990.0	0.0025	0.00109	0.066	0.064	2
9	0.29	876	996.0	0.12	0.000958	0.16	0.22	34
10	0.30	865	996.0	0.035	0.000958	0.18	0.22	20
11	0.32	843	996.0	0.016	0.000958	0.21	0.22	4
12	0.35	822	996.0	0.0067	0.000958	0.22	0.22	1
13	0.11	871	996.0	0.00054	0.000958	0.32	0.38	20
14	0.14	871	990.0	0.00054	0.00104	0.26	0.30	16
15	0.14	870	996.0	0.00055	0.000958	0.26	0.30	15

TABLE 5. Comparison of the calculated jetting velocity with the experimental values of Scheele & Meister.

by Scheele & Meister and the column $\tilde{V}_J$ presents the results given by (5.7). The error between V_{JSM} and $\tilde{V}_J$ is presented in the last column of the table. As one would have expected, in all the cases where the viscosity of the fluids (μ_1 or μ_2) is important, the error of our model is also significant. This is because in the equation of motion (5.1), viscosity effects are not considered. In all other cases, the error is confined to a few percent as was the case with our measurements.

5.2. *Validity domain of the model*

In the model presented above, we did not consider the acceleration of the feeder jet due to gravity. This leads to the paradox that at one point the drop moves faster than the feeder jet. From (5.4), this critical point is reached at $t^* = t_{max}/2 + \tilde{V}_0/\gamma > t_{max}/2$. Equation (5.4) is thus only valid in the domain $t \in [0, t^*]$.

A more complete model would consider the acceleration of the feeding jet. This model is presented in figure 18. To simplify the discussion, the wetting effects are not considered in this paragraph, so that only the diameter, D, enters the equations. The conservation of mass and energy in the feeder jet leads to the following velocity field:

$$\tilde{V}_{0z} = \tilde{V}_0 \left[1 + \frac{2gh}{V_0^2}(1 - z/h)\right]^{1/2}, \quad \text{where} \quad \tilde{V}_{0z} = |V_0(z)| \quad \text{and} \quad \tilde{V}_0 = |V_0(h)|, \quad (5.9)$$

Defining the Froude number as $Fr = 2gh/V_0^2$ and the function $X(z) = [1 + Fr(1 - z/h)]^{1/2}$, equation (5.9) simply becomes $\tilde{V}_{0z} = \tilde{V}_0 X(z)$. Considering the dynamics of the 'lump' as shown in figure 18, the conservation of mass and momentum, applied to the 'lump', leads to

$$\mathrm{d}M/\mathrm{d}t = \rho s(z)[\tilde{V}_{0z} + v(z)], \quad (5.10)$$

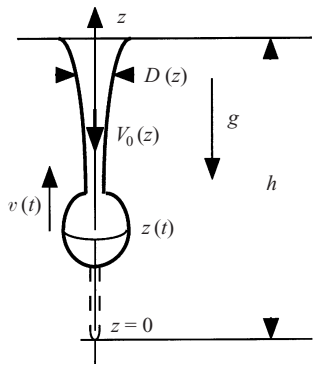

FIGURE 18. Sketch for the dynamics of a pending drop when the feeding jet is accelerated by gravity.

and

$$\mathrm{d}(Mv)/\mathrm{d}t = Mg - \pi D(z)\sigma + \rho s(z)\tilde{V}_{0z}[\tilde{V}_{0z} + v(z)], \tag{5.11}$$

where $s(z)$, $D(z)$ and $v(z)$, respectively stand for the jet cross-section, the jet diameter and the lump velocity at the location z. From the conservation of mass in the jet, $s(z)/S = X(z)^{-1}$ and $D(z)/D = X(z)^{-1/2}$. Introducing dimensionless variables as $z^* = zD/(2a^2)$, $v^* = v/\tilde{V}$, $t^* = tD\tilde{V}/(2a^2)$, and $M^* = M/(\rho S 2a^2/D)$, one gets the following form for the system to be solved:

$$\frac{\mathrm{d}M}{\mathrm{d}t} = \frac{We^{1/2}}{2} + \frac{v}{X(z)}, \tag{5.12}$$

$$\frac{\mathrm{d}Mv}{\mathrm{d}t} = -M + X(z)^{1/2} - \frac{We^{1/2}}{2}\left(v + \frac{We^{1/2}}{2}X(z)\right), \tag{5.13}$$

$$X(z) = \left[1 + Fr\left(1 - \frac{8z}{FrWe}\right)\right]^{1/2}, \tag{5.14}$$

where $We \equiv \rho V_0^2 D/\sigma$ and where the asterisks have been dropped in the notation of the dimensionless variables. The unknowns being $v(t)$ and $M(t)$, the system (5.12), (5.13) and (5.14) must satisfy the initial conditions $z(t = 0) = M(t = 0) = 0$. This allows the direct integration of the mass conservation equation (5.12), using $v = \mathrm{d}z/\mathrm{d}t$:

$$M(z,t) = \frac{We^{1/2}}{2}t + \frac{We}{4}(X(0) - X(z)). \tag{5.15}$$

In the limit $Fr \to 0$, this expression for the mass of the lump reduces to (5.2). The limit $M = 0$ in (5.13) gives the initial value of the velocity $v(0) = X(0)^{1/4} - X(0)We^{1/2}/2$. This value allows the numerical integration of (5.13), using (5.15) and (5.14).

To obtain the influence of the acceleration of the feeder jet on the transition, using our model, the free parameter, h, in the above description is taken as the distance travelled during the necking time τ_n:

$$\int_o^h \frac{\mathrm{d}z}{\tilde{V}_{0z}} = \tau_n, \tag{5.16}$$

the solution of which,

$$Fr = (1 + g\tau_n/V_0)^2 - 1, \tag{5.17}$$

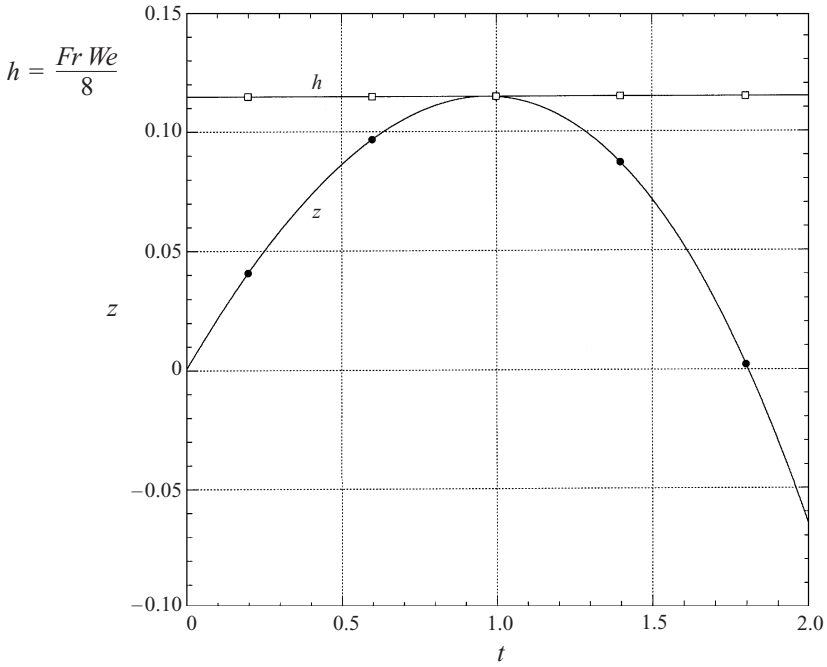

FIGURE 19. Numerical integration of the 'lump' trajectory obtained with $Bo = 0.4$ and $We = 1.813$ (corresponding to $Fr = 0.50$).

relates the Froude number to the dimensionless parameter, $g\tau_n/V_0$, which evaluates the gravity effect during the necking time. In the small Froude number limit, this solution is simply $h = V_0\tau_n$ as previously used in the model. Taking $\tau_n = 3.16[\rho D(z)^3/(8\sigma)]^{1/2}$ in (5.17) allows the integration of the system with time as shown in figure 19. For each Bond number, the transition is defined as the critical Weber number for which the maximum value of z corresponds to $h \equiv WeFr/8$ (according to figure 19, We_c (0.4) = 1.813). The numerical solution of this problem is presented in figure 20 and compared to the model which, following (5.8), can be written in this case as

$$We_c = \left[1 + KBo^2 - \left(\left(1 + KBo^2\right)^2 - 1\right)^{1/2}\right]^2 \quad \text{with} \quad K \approx 0.37. \tag{5.18}$$

The agreement between the model and the numerical integration is within 10% for Bond numbers $Bo \leqslant 0.5$ that correspond to Froude numbers $Fr \leqslant 1$ and stays within 20% for Bond numbers $Bo \leqslant 1$ that correspond to Froude numbers, $Fr \leqslant 5.3$. Observe from tables 4 and 5 that the model is accurate for all the data presented.

5.3. *Discussion of the model*

(i) On the effect of gravity, we observe from figure 20 that an increase of g and thus of Bo contributes to a decrease in the critical Weber number. In the limit of zero gravity ($Bo = 0$), the transition velocity becomes $\tilde{V}$ and the critical Weber number is $We_c = 4Bo_o/Bo = 4D_0/D$ (equation (5.8)).

(ii) Concerning the hysteresis observed between the transitions $PD \rightarrow J$ and $J \rightarrow PD$ for $D \approx a$, this model provides some physical insight on its origin. Considering figure 20, we observe that the critical Weber number, $We_c \equiv \rho\tilde{V}_J^2 D/\sigma$, decreases as the Froude number, $Fr = 2gh/\tilde{V}_J^2$, is increased. Since h is smaller for $PD \rightarrow J$ than for $J \rightarrow PD$, one deduces that the transition from $J \rightarrow PD$ occurs at a smaller We_c than

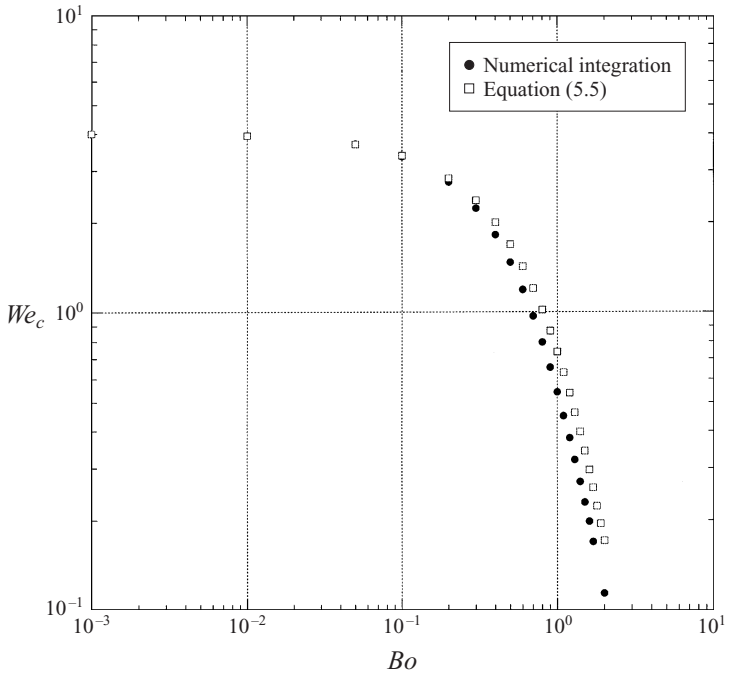

FIGURE 20. The critical Weber number We_c as a function of the Bond number and comparison with the model.

the transition from $PD \rightarrow J$. Since the hysteresis effect is related to gravity it should not be observed in the limit $g = 0$. This explains why the hysteresis is only observed for the larger diameters where the Bond number comes closer to 1. For the smaller diameters, gravity is negligible and the critical Weber number $We_c = 4Bo_o/Bo$ is reached.

6. Conclusion

We extended the Taylor model for a recessing liquid edge to account, in the inviscid limit, for gravitational and inertia effects. This model provides a criterion for the transition from dripping to jetting when a Newtonian fluid is injected vertically downwards into stagnant air. This model clearly identifies the roles of gravity, inertia and surface tension. It also provides an understanding of the physical origin of the hysteresis observed between the transitions dripping/jetting and jetting/dripping. Predictions of the jetting velocities using this model are shown to be in good agreement with existing measurements as well as with new experimental evidence. This model is obtained in the inviscid limit and a natural extension of this work would be the consideration of the viscous effects.

We thank Amable Liñan and Alberto Verga for critically reading the original version of this paper. Their remarks and suggestions, as well as stimulating discussions, lead to the improvement of the final version of this paper. We also thank Guillaume Préaux and Carlos Martinez for the assistance they provided with some of the measurements. This work was partly supported by a grant from the ONR N0014-96-1-0213.

REFERENCES

Chesters, A. K. 1977 An analytic solution for the profile and volume of a small drop or bubble symmetrical about a vertical axis. *J. Fluid Mech.* **81**, 609–624.

Clift, R., Grace, J. R. & Weber, M. E. 1978 *Bubbles, Drops, and Particles.* Academic.

D'Innocenzo, A. & Renna, L. 1996 Dripping faucet. *Intl J. Theor. Phys.* **35**, 941–973.

Eggers, J. & Dupont, T. F. 1994 Drop formation in a one-dimensional approximation of the Navier–Stokes equation. *J. Fluid Mech.* **262**, 205–221.

Harkins, W. D. & Brown, F. E. 1919 The determination of surface tension (Free surface energy), and the weight of falling drops: the surface tension of water and benzene by the capillary height method. *J. Am. Chem. Soc.* **41**, 499–524.

Kumar, R. 1971 A unified approach to bubble and drop formation. *Chem. Engng Sci.* **26**, 177–184.

Landau, L. & Lifchitz, E. 1971 *Physique Théorique: Mécanique des Fluides.* Mir.

Le Dizès, S. 1997 Global modes in falling capillary jets. *Eur. J. Mech.* B/*Fluids* **16**, 761–778.

Limat, L., Jenfer, P., Dagens, B., Touron, E., Fermigier, M. & Wesfreid, J. E. 1992 Gravitational instabilities of thin liquid layers: dynamics of pattern selection. *Physica* D **61**, 166–182.

Longuet-Higgins, M. S., Kerman, B. R. & Lunde, K. 1991 The release of air bubbles from an underwater nozzle. *J. Fluid Mech.* **230**, 365–390.

McCarthy, M. J. & Molloy, N. A. 1974 Review of stability of liquid jets and the influence of nozzle design. *Chem. Engng J.* **7**, 1–20.

Martien, P., Pope, S. C., Scott, P. L. & Shaw, R. S. 1985 The chaotic behaviour of the leaky faucet. *Phys. Lett.* **110A**, 399–404.

Michael, D. H. 1981 Meniscus stability. *Ann. Rev. Fluid Mech.* **13**, 189.

Monkewitz, P. A. 1990 The role of absolute and convective instability in predicting the behaviour of fluid systems. *Eur. J. Mech.* B/*Fluids* **9**, 395–413.

Padday, J. F. & Pitt, A. R. 1973 The stability of axisymmetric menisci. *Phil. Trans. R. Soc. Lond.* A **275**, 489–527.

Plateau, J. 1873 *Statique Expérimentale et Théorique des Liquides.* Gauthier-Villars et C^{ie}.

Rayleigh, Lord 1879*a* On the instability of jets. *Proc. Lond. Math. Soc.* **10**, 4–13.

Rayleigh, Lord 1879*b* *Proc. R. Soc. Lond.* A **29**, 71.

Rayleigh, Lord 1892 On the instability of cylindrical fluid surfaces. *Phil. Mag.* **34**, 177–180.

Rayleigh, Lord 1899 Investigations in capillarity: the size of drops. – The liberation of gas from supersaturated solutions. – Colliding jets. – The tension of contaminated water-surfaces. – A curious observation. *Phil. Mag.* **48**, 321–337.

Rayleigh, Lord 1915 The principle of similitude. *Nature* **95**, 66–68.

Savart, F. 1833 Mémoire sur la constitution des veines liquides lancées par des orifices circulaires en mince paroi. *Ann. Chim.* **53**, 337–386.

Scheele, G. F. & Meister, B. J. 1968*a* Drop formation at low velocities in liquid-liquid systems. *AIChE J.* **14**, 9–15.

Scheele, G. F. & Meister, B. J. 1968*b* Prediction of jetting velocity. *AIChE J.* **14**, 15–19.

Smith, S. W. J. & Moss, H. 1917 Experiments with mercury jets. *Proc. R. Soc. Lond.* A **43**, 373–393.

Tate, T. 1864 On the magnitude of a drop of liquid formed under different circumstances. *Phil. Mag.* **27**, 176–180.

Taylor, G. I. 1959 The dynamics of thin sheets of fluid. III. Disintegration of fluid sheets. *Proc. R. Soc. Lond.* A **253**, 313–321.

Tyler, E. & Richardson, E. G. 1925 The characteristic curves of liquid jets. *Proc. Phys. Soc.* **37**, 297–311.

Tyler, E. & Watkin, F. 1932 Experiments with capillary jets. *Phil. Mag.* **14**, 849–881.

White, J. L. & Ide, Y. 1975 Rheology and dynamics of fiber formation from polymer melts. *Appl. Polym. Symp.* **27**, 61–102.

Wilkinson, M. C. 1972 Extended use of, and comments on, the drop-weight (drop-volume) technique for the determination of surface and interfacial tensions. *J. Colloid Interface Sci.* **40**, 14–26.

Wilson, S. D. R. 1988 The slow dripping of a viscous fluid. *J. Fluid Mech.* **190**, 561–570.

Zhang, X. & Basaran, O. A. 1995 An experimental study of dynamics of drop formation. *Phys. Fluids* **7**, 1184–1203.